

Condensation of collective polar vortex modesTiannan Yang ^{1,*}, Cheng Dai,¹ Qian Li ², Haidan Wen,³ and Long-Qing Chen ^{1,†}¹*Department of Materials Science and Engineering, The Pennsylvania State University, University Park, Pennsylvania 16802, USA*²*State Key Laboratory of New Ceramics and Fine Processing, School of Materials Science and Engineering, Tsinghua University, Beijing 100084, China*³*Advanced Photon Source, Argonne National Laboratory, Lemont, Illinois 60439, USA*

(Received 7 December 2020; accepted 4 June 2021; published 15 June 2021)

The dynamics of extended objects such as domain walls, domain bubbles, vortex structures, etc., can be described by their equations of motion associated with their effective mass and spring constant. Here we analytically derive the equations of motion for the polarization dynamics and elastodynamics for the structural responses of ferroelectric polar vortices, and theoretically extract their effective mass, spring constant, and mode frequencies. We demonstrate two subterahertz phonon modes and predicted their frequencies, both consistent with our recent experimental measurements and phase-field simulations. We show that elastic modulation of the energy function and spring constants leads to a condensation of a collective mode upon a second-order structural transition from symmetric to asymmetric vortices at a critical strain, analogous to the ferroelectric soft phonon mode at a ferroelectric transition. The present work offers a theoretical framework for predicting and manipulating the ultrafast collective dynamics of polar nanostructures.

DOI: [10.1103/PhysRevB.103.L220303](https://doi.org/10.1103/PhysRevB.103.L220303)

Ferroelectric polar nanostructures including domains and domain walls show structural oscillation modes extending to subterahertz frequencies and beyond [1–7], significantly higher than that of magnetic domain structures, which is typically around gigahertz [8,9], making them promising candidates for high-frequency electronic applications. Unlike magnetic domain structures that are made up of spins, ferroelectric domain structures develop through arrangements of electric dipoles, thus giving rise to substantially different dynamical behaviors [10]. Understanding the high-frequency dynamics of polar nanostructures is essential to both their fundamental physics and practical applications.

Recently, novel topological nanostructures including polar vortices [11] and polar skyrmions [12] have been discovered in layered oxide superlattices. For example, as shown in Fig. 1(a), in a $(\text{PbTiO}_3)_{16}/(\text{SrTiO}_3)_{16}$ superlattice thin film, periodic arrays of polar vortex tube pairs of opposite rotation directions are formed within the ferroelectric PbTiO_3 layers. These polar topological structures have a spatial scale of <10 nm at room temperature, smaller than their nominal magnetic counterparts [13,14]. Such extended objects (i.e., domain walls, skyrmions, vortices, etc.) can host collective dynamics of coherent motions over multiple unit cells. Indeed, we have very recently observed subterahertz phonon modes unique to polar vortices, in which a specific mode attributed to the motion of vortices exhibits a softening of the frequency around a mesoscale structural transition at a critical strain, based on a combination of terahertz-field pump, x-ray

diffraction probe experiment, and atomistic and phase-field simulations [15].

For studying the dynamics of nanostructures, the ability to analytically describe their equations of motion [16–26] is extremely useful for analyzing the underlying mechanisms and notable factors that dominate the dynamics. In this Letter, we present a theoretical study of two sub-terahertz modes of polar vortices in ferroelectric superlattices, where we analytically derive the equation of motion for the vortex modes based on coupled polarization dynamics and elastodynamics, and extract the effective mass and spring constant. By establishing the energetics of the system, we discover a strain modulation of the spring constant of a structural mode, which causes the transition between symmetric and asymmetric vortices as well as condensation of the mode frequency. The analytically predicted mode frequencies are in good agreement with the experiment and simulations reported in [15].

Figure 1(b) presents a schematic of the proposed model for the polar vortices. The polarization profile of each vortex within the ferroelectric material can be approximated by an ensemble of four domain-like regions with each possessing nearly homogeneous polarization along in-plane ($\pm x_1$) or out-of-plane ($\pm x_3$) directions, forming a closed polarization vortex. Adjacent in-plane and out-of-plane domain-like regions are connected through domain-wall-like regions possessing a 90° polarization rotation, which are in a 45° angle with the film plane for a charge-neutral condition. For vortices with a vertical dimension d larger (or smaller) than its horizontal dimension a , two neighboring out-of-plane (or in-plane) domain-like regions with antiparallel polarizations will also border each other forming a 180° domain-wall-like region, where the vortex core is located at the center of the region. According to atomistic simulations [15], the vortex

*tuy123@psu.edu

†lqc3@psu.edu

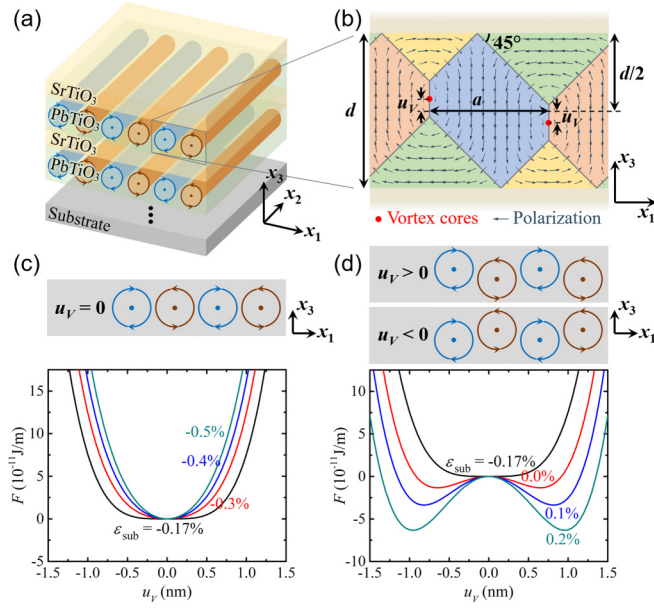


FIG. 1. (a) Schematic of the polar vortex array in a ferroelectric superlattice thin film. The circular arrows indicate the polarization direction of the vortex tubes. (b) Schematic of the analytical model showing the x_1 - x_3 cross section of the ferroelectric layer, containing a pair of polar vortices with opposite rotation directions. Several domain-like regions each containing nearly homogeneous polarization are shaded with different colors. (c), (d) Top panels show schematics of symmetric and staggered vortices, and bottom panels show free energy of the polar vortices as a function of u_V under different substrate strains, with (c) $\varepsilon_{\text{sub}} \leq \varepsilon_C$ and (d) $\varepsilon_{\text{sub}} > \varepsilon_C$, respectively.

cores may undergo vertical displacements u_V away from the center plane of the ferroelectric layer, either spontaneously or under external stimuli, while maintaining the charge-neutral condition, with neighboring vortices of opposite rotation directions adopting opposite displacements. The dimensional parameters d , a , and u_V provide a complete description of the vortex structure. u_V may respond to external stimuli or condition variations, while d and a are fixed due to confinement by the dimensions of the film. The dielectric SrTiO₃ layers are assumed to have a negligible polarization compared with that of the ferroelectric layers.

We first establish the thermodynamics of the system by formulating a potential energy as a function of u_V and study the equilibrium state of the vortices under given conditions. A similar approach has been employed in studying static properties of domain walls [27]. The potential energy includes bulk, gradient, elastic, and electrostatic energy contributions. The total bulk and gradient energies can be approximated as $F_{\text{bulk-gradient}} = F_{\text{SD}} + F_W$, where F_{SD} is the bulk energy of a stable single domain state and F_W is the domain wall energy. F_W is determined by the lengths of domain-wall-like regions, with a total of $2(d-a)$ and $4\sqrt{2}a$ for 180° and 90° domain-wall-like regions, respectively, both independent of u_V . Therefore, $F_{\text{bulk-gradient}}$ is a constant independent of u_V .

The elastic energy is separated into two parts, corresponding to a decomposition of the strain ε into spatially homogeneous and inhomogeneous parts, i.e., $\varepsilon(\mathbf{x}) = \bar{\varepsilon} +$

$\delta\varepsilon(\mathbf{x})$. The homogeneous part is given by

$$F_{\text{elastic}}^{\text{hom}} = \frac{1}{2} S \left(c_{11} - \frac{c_{12}^2}{c_{11}} \right) (\varepsilon_{\text{sub}} - \bar{\varepsilon}_1^0)^2, \quad (1)$$

under an in-plane strain ε_{sub} due to substrate clamping and a relaxed out-of-plane stress. Here $S = 2ad$ is the total area of the vortex pair, \mathbf{c} is the elastic stiffness tensor, and $\bar{\varepsilon}_1^0$ is the average eigenstrain given by

$$\bar{\varepsilon}_1^0 = \frac{S_{\text{IP}} Q_{11} P_S^2 + (S - S_{\text{IP}}) Q_{12} P_S^2}{S}. \quad (2)$$

Q is the electrostrictive coefficient, and $S_{\text{IP}} = a^2 + 4u_V^2$ is the total area of the in-plane domain-like regions. The exact inhomogeneous elastic energy cannot be analytical calculated, but it can be approximated as a power series of u_V with only even orders due to a mirror symmetry about the central plane of the ferroelectric layer. For simplicity, it is approximated with the two leading orders,

$$F_{\text{elastic}}^{\text{inhom}} = A_0 + A_2 u_V^2. \quad (3)$$

The coefficients A_0 and A_2 are determined by material properties and vortex dimensions, and they can be obtained through fitting the numerically calculated elastic energies with different u_V to Eq. (3) (see Note S1 of the Supplemental Material [28]).

Since the polarization field forms closed loops with zero bound charges, the system possesses negligible electrostatic energy. We find that the closed loop configuration is well protected due to the minimization of electrostatic energy, with details given in Note S2 of the Supplemental Material [28]. It is thus found that the energy for the vortex displacement is dominated by the elastic contribution.

Summing up the energy contributions, the total potential energy adopts a fourth-order polynomial of u_V ,

$$F(u_V) = \frac{1}{2} K_2 u_V^2 + \frac{1}{4} K_4 u_V^4, \quad (4)$$

with u_V -independent terms omitted. The linear and third-order spring constants K_2 and K_4 are given by

$$K_2 = K_{2\varepsilon} (\varepsilon_C - \varepsilon_{\text{sub}}), \quad (5)$$

$$K_{2\varepsilon} = 8P_S^2 \left(c_{11} - \frac{c_{12}^2}{c_{11}} \right) (Q_{11} - Q_{12}), \quad (6)$$

$$\varepsilon_C = \left[\frac{a}{2d} (Q_{11} - Q_{12}) + Q_{12} \right] P_S^2 + \frac{2A_2}{K_{2\varepsilon}}, \quad (7)$$

$$K_4 = \frac{16P_S^4}{ad} \left(c_{11} - \frac{c_{12}^2}{c_{11}} \right) (Q_{11} - Q_{12})^2. \quad (8)$$

For PbTiO₃/SrTiO₃ superlattice thin films, $d = 6.4$ nm, $a = 5.0$ nm [11], $c_{11} = 180$ GPa, $c_{12} = 80$ GPa [29], $Q_{11} = 0.089$ C⁻²m⁴, $Q_{12} = -0.026$ C⁻²m⁴, $P_S = 0.75$ C m⁻² [30], and $A_2 = -4.6 \times 10^8$ J m⁻³. We obtain $K_{2\varepsilon} = 7.5 \times 10^{10}$ J m⁻³, $\varepsilon_C = -0.17\%$, $K_4 = 3.0 \times 10^{26}$ J m⁻⁵.

Equation (4) exhibits either a single- or double-well potential depending on the sign of K_2 , which is further controlled by the substrate strain ε_{sub} . Similarly to the description of phase transitions in the Landau theory, Eq. (4) indicates the emergence of a spontaneous u_V at the critical strain ε_C . For $\varepsilon_{\text{sub}} \leq \varepsilon_C$, $K_2 \geq 0$, the energy function contains a single stable state

at $u_V = 0$, with a deeper energy well under more compressive strains [Fig. 1(c)] due to the increased energy penalty in forming in-plane domain-like regions. For $\varepsilon_{\text{sub}} > \varepsilon_C$, $K_2 < 0$, the system becomes intrinsically unstable at $u_V = 0$, while a spontaneous displacement of the vortex cores is induced with two degenerate states following $u_{V0} = \pm\sqrt{-K_2/K_4}$, which increases upon increasing the tensile strain [Fig. 1(d)]. This leads to a second-order phase transition of the polar structure from symmetric vortices ($u_V = 0$) to asymmetric ones with a staggered arrangement ($u_V \neq 0$), as illustrated by the top panels of Figs. 1(c) and 1(d). This phenomenon is consistent with the strain-induced structural transition found by atomistic simulations [15]. Here our analysis demonstrates the emergence of staggered vortices as a structural adaptation to release the elastic energy under suitable mechanical conditions.

We next study the dynamics of the polar vortices and derive their equation of motion. Two experimentally characterized subterahertz phonon modes, i.e., the slow mode and the fast mode, are investigated. Following atomistic simulations [15], the slow mode represents the collective motion of the vortices with vortex cores oscillating vertically around the equilibrium positions, as shown in Fig. 2(a). From the thermodynamic analysis above, it is now clear that the main restoring force of the mode comes from the elastic energy contribution.

The slow mode can be described by the equation of motion of u_V . The kinetic energy of vortex motion includes contributions from polarization dynamics and elastodynamics. The polarization dynamics follows [31,32]

$$\mu\ddot{\mathbf{P}} + \gamma\dot{\mathbf{P}} + \frac{\delta F}{\delta \mathbf{P}} = 0, \quad (9)$$

where μ and γ are the effective mass and damping coefficient of polarization evolution, respectively. The corresponding kinetic energy is given by

$$E_{k,P} = \int \frac{1}{2} \mu \dot{\mathbf{P}}^2 dx_1 dx_3. \quad (10)$$

Since the polarization inhomogeneity mostly lies around the domain-wall-like regions, for vertical motion of the vortices, 90° domain-wall-like regions show the strongest polarization response $\dot{\mathbf{P}}$ [see the $\Delta\mathbf{P}$ profile in Fig. 2(a)]. $E_{k,P}$ can be calculated by estimating the contribution of these regions only, i.e., $E_{k,P} \approx \frac{1}{2} \mu \dot{P}_W^2 S_W$, where \dot{P}_W is the spatially averaged rate of polarization change inside the 90° domain-wall-like regions, and S_W is the total area of these regions with $S_W = 4\sqrt{2}aw$, assuming a domain wall width of w . Within these regions where polarization rotates between in-plane and out-of-plane states, the average polarization gradient is $\sqrt{2}P_S/w$. For these regions moving vertically with a velocity $\dot{\mathbf{u}}_V$ at a 45° angle to the polarization gradient, we write $\dot{P}_W = (\sqrt{2}P_S/w) \times \dot{u}_V \times \cos 45^\circ = P_S \dot{u}_V / w$. It shows that the kinetic energy of polarization within the vortex pair resembles that of an object,

$$E_{k,P} = \frac{1}{2} m_P \dot{u}_V^2, \quad (11)$$

with an effective mass of $m_P = 4\sqrt{2}\mu P_S^2 a/w$. For PbTiO_3 , $w = 2.1$ nm [33], $\mu = 7.53 \times 10^{-17}$ J A $^{-2}$ m, $\gamma = 2.0 \times 10^{-7}$ J A $^{-2}$ m s $^{-1}$ [15]. We obtain $m_P = 5.7 \times 10^{-16}$ kg m $^{-1}$.

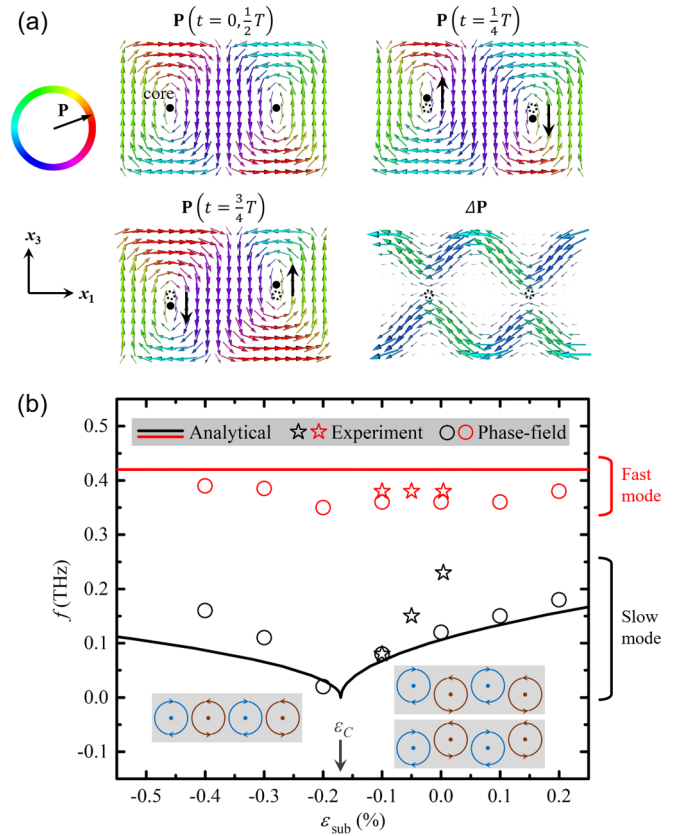


FIG. 2. (a) Polarization field \mathbf{P} at times $t = 0, T/4, T/2, 3T/4$ within an oscillation period of the slow mode and oscillation amplitude $\Delta\mathbf{P} = \mathbf{P}(T/4) - \mathbf{P}(0)$. The color arrows represent \mathbf{P} or $\Delta\mathbf{P}$, with the color indicating the direction shown by the color wheel. The solid and dashed circles represent the current and equilibrium positions of vortex cores, respectively. The black arrows indicate the direction of the core displacement. (b) Mode frequencies as a function of the substrate strain from the analytical model and those from experiment and phase-field simulation [15]. Bottom insets show the equilibrium states with symmetric and staggered vortices.

The kinetic energy for elastodynamics is given by

$$E_{k,\text{elastic}} = \int \frac{1}{2} \rho \dot{\mathbf{u}}^2 dx_1 dx_3, \quad (12)$$

where ρ is the material density and \mathbf{u} is the lattice displacement. Similarly to $E_{k,P}$, $E_{k,\text{elastic}}$ can be approximated as $E_{k,\text{elastic}} \approx \rho \dot{u}_W^2 S_W / 2$, with \dot{u}_W^2 the average square velocity of lattice motion inside the 90° domain-wall-like regions. We estimate that $\dot{u}_W^2 = (Q_{11} - Q_{12})^2 P_S^4 \dot{u}_V^2 / 24$, with derivations provided in Note S3 of the Supplemental Material [28]. It then follows that

$$E_{k,\text{elastic}} = \frac{1}{2} m_{\text{elastic}} \dot{u}_V^2 \quad (13)$$

with $m_{\text{elastic}} = \sqrt{2}\rho(Q_{11} - Q_{12})^2 P_S^4 aw / 6$ the effective mass. $\rho = 7.52 \times 10^3$ kg m $^{-3}$ for PbTiO_3 , and $m_{\text{elastic}} = 7.8 \times 10^{-17}$ kg m $^{-1}$. Since $m_P \gg m_{\text{elastic}}$, the slow mode is dominated by polarization dynamics. The total kinetic energy of the vortex pair is given by

$$E_k = E_{k,P} + E_{k,\text{elastic}} = \frac{1}{2} m_V \dot{u}_V^2 \quad (14)$$

with $m_V = m_P + m_{\text{elastic}} = 6.5 \times 10^{-16} \text{ kg m}^{-1}$. Thus, the effective mass of each vortex tube is $3.2 \times 10^{-16} \text{ kg m}^{-1}$.

Based on the kinetic and potential energy functions [Eqs. (4) and (14)], the equation of motion of the vortex core is given by

$$m_V \ddot{u}_V + K_2 u_V + K_4 u_V^3 = 0 \quad (15)$$

with energy dissipation neglected. It describes an anharmonic oscillator, yet for small perturbations (i.e. $|\Delta u_V| \ll \sqrt{K_2/K_4}$) analytical solutions can be derived with harmonic approximations. For $\varepsilon_{\text{sub}} \leq \varepsilon_C$, the spring constant $K_2 \geq 0$ and the vortices oscillate around the equilibrium point at $u_{V0} = 0$ (i.e., symmetric vortices). After neglecting the u_V^3 term under small perturbations, Eq. (15) gives rise to a harmonic oscillator with a frequency f dependent on the substrate strain ε_{sub} , i.e.,

$$u_V(t) = u_{VA} \sin(2\pi f t), \quad (16)$$

$$f = \frac{1}{2\pi} \sqrt{\frac{K_2}{m_V}} = \frac{1}{2\pi} \sqrt{\frac{K_{2\varepsilon}(\varepsilon_C - \varepsilon_{\text{sub}})}{m_V}}. \quad (17)$$

As shown in Fig. 2(b), the slow mode frequency decreases with increasing ε_{sub} and approaches zero at $\varepsilon_{\text{sub}} = \varepsilon_C$ (i.e., spring constant $K_2 = 0$). Such mode condensation at ε_C signals a reduced structural stability of the symmetric vortices upon approaching a transition to staggered vortices, which is analogous to the condensation of the soft phonon mode for a ferroelectric phase transition at the Curie temperature [34,35]. Further increasing the substrate strain to $\varepsilon_{\text{sub}} > \varepsilon_C$ (spring constant $K_2 < 0$) results in an imaginary nominal frequency from Eq. (17), indicating the intrinsic instability of the symmetric vortices, accompanied by the transition to the staggered vortices with two new equilibrium core positions at $u_{V0} = \pm\sqrt{-K_2/K_4}$. Through expansion around the new u_{V0} , Eq. (15) is reformulated as

$$m_V \ddot{u}_V - 2K_2(u_V - u_{V0}) \pm 3\sqrt{-K_2 K_4}(u_V - u_{V0})^2 + K_4(u_V - u_{V0})^3 = 0, \quad (18)$$

with a new linear spring constant of $-2K_2$. Through neglecting second- and third-order terms, the harmonic solution for small perturbations is given by

$$u_V(t) = u_{VA} \sin(2\pi f t) + u_{V0}, \quad (19)$$

$$f = \frac{1}{2\pi} \sqrt{\frac{-2K_2}{m_V}} = \frac{1}{2\pi} \sqrt{\frac{2K_{2\varepsilon}(\varepsilon_{\text{sub}} - \varepsilon_C)}{m_V}}. \quad (20)$$

The mode frequency rises with increasing substrate strain due to the increased spring constant indicating a higher stability of the staggered vortices. As a result, the mode frequency shows a minimum of $f = 0$ at $\varepsilon_{\text{sub}} = \varepsilon_C$ while it rises going towards both tensile and compressive strain sides of ε_C , with symmetric and staggered vortices, respectively [see Fig. 2(b)].

The oscillation amplitude u_{VA} is determined by the energy input upon mode excitation. With an increased amplitude beyond the small perturbation regime, the mode frequency will increase for symmetric vortices due to the additional third-order restoring force terms [Eq. (15)] of the anharmonic oscillator. For the staggered vortices, it is further noted that

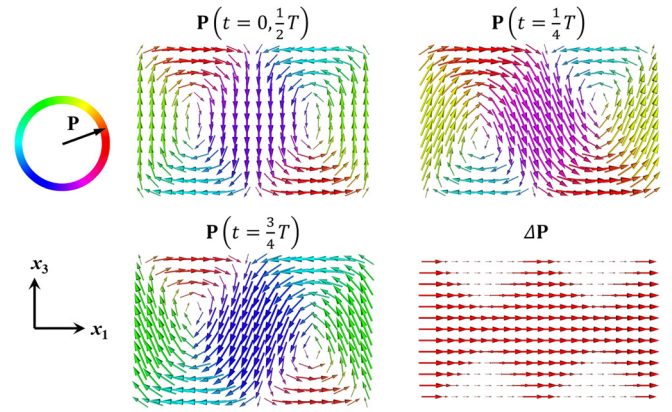


FIG. 3. Polarization field \mathbf{P} at times $t = 0, T/4, T/2, 3T/4$ within an oscillation period of the fast mode and amplitude $\Delta\mathbf{P} = \mathbf{P}(T/4) - \mathbf{P}(0)$. The arrows represent \mathbf{P} or $\Delta\mathbf{P}$, with the color indicating the direction shown by the color wheel.

with sufficient energy input, the oscillator will be able to pass the energy barrier at $u_V = 0$ between the two degenerate states with $u_{V0} = \pm\sqrt{-K_2/K_4}$ and transition between them. Numerical solutions of the anharmonic oscillator are provided in Note S4 of the Supplemental Material [28].

The strain-dependent frequencies of the slow vortex mode predicted by the analytical model agree well with the experiment and phase-field simulations in [15], as presented in Fig. 2(b). We conclude that the soft mode is dominated by the proposed structural dynamics rather than other processes, e.g., electron dynamics. The slightly smaller analytical frequency on the compressive strain side compared with phase-field simulation is due to the small perturbation assumption. The slow mode identified in the phase-field simulation also demonstrates a vortex motion similar to that in the analytical model, as shown in Note S5 of the Supplemental Material [28].

In addition to the slow mode, the polar vortices also host a fast mode experimentally found at $\sim 0.38 \text{ THz}$ [15]. This can be attributed to the structural response with polarization in all regions oscillating in phase without changing the geometry and location of each region, which corresponds to a localized ferroelectric soft phonon mode. The spatial polarization profile of the fast mode with in-plane polarization responses is shown in Fig. 3. The out-of-plane domain-like regions show a larger amplitude than do the in-plane domain-like regions due to the stronger dielectric constant κ_{11} perpendicular to the polarization than that parallel to it. The restoring force of the mode lies in the dielectric response. For small perturbations within a range of linear dielectric constant, we consider the polarization oscillation within the out-of-plane domain-like regions subject to a linear restoring force of $-\delta F/\delta P_1 = -P_1/\kappa_0\kappa_{11}$, κ_0 being the vacuum permittivity. The polarization dynamics Eq. (9) is rewritten as

$$\mu \ddot{P}_1 + \gamma \dot{P}_1 + \frac{P_1}{\kappa_0\kappa_{11}} = 0. \quad (21)$$

The mode does not couple with the elastic field since the piezoelectric coefficient $d_{11} = d_{13} = 0$ with an out-of-plane polar axis. Equation (21) describes a damped harmonic

oscillator with a frequency of

$$f = \frac{1}{2\pi} \sqrt{\frac{1}{\kappa_0 \kappa_{11} \mu} - \frac{\gamma^2}{4\mu^2}}. \quad (22)$$

$f = 0.42$ THz for PbTiO_3 (with $\kappa_{11} = 210$ [30]), independent of the substrate strain. The predicted fast mode frequency also matches our experiment and phase-field simulations, as presented in Fig. 2(b).

Polar vortices may also host other collective dynamics which possibly include in-plane oscillation of vortex cores as well as rotation and deformation of vortices, etc. These motions have higher energy costs due to the electrostatic energy penalty from breaking the closed polarization loop and therefore should show weaker amplitudes or higher frequencies, which is consistent with the experimental observation of the slow mode being the only notable phonon mode in the lower frequency range ($f < 0.3$ THz) and the observation of several additional frequency peaks with higher frequencies ($f > 0.5$ THz) by atomistic and phase-field simulations [15]. These modes are neglected in the present works but can be further described by allowing additional degrees of freedom of the system.

In summary, we develop an analytical framework for modeling new collective dynamics in polar vortices. By establishing the energy functions of the polar structure, we theoretically examine the subterahertz phonon modes in $\text{PbTiO}_3/\text{SrTiO}_3$ superlattices discovered by pump-probe experiments [15]. The slow mode of the vortex motion is analogous to the motion of a massive object connected to a nonlinear spring, similar to magnetic vortices [18,36]. However, unlike the rotational modes found in magnetic vortices [36,37], the ferroelectric vortex mode shows linear motions of vortex cores, due to the different dynamics of electric dipoles

from that of spins. The mode frequency can be effectively tuned by strain, as a result of the elastic modulation of the potential energy function and the effective spring constants of the vortex motion. This also leads to a condensation of the mode frequency around a mesoscale structural transition from symmetric to staggered vortices at a critical strain, similar to the condensation of the soft phonon mode in ferroelectric materials at the Curie temperature. The fast mode is an optical phonon mode representing localized oscillation of polarization with fixed vortex positions, which is decoupled from strain. The present approach for deriving the equations of motion by establishing the energetics, based on fundamental thermodynamics, polarization dynamics, and elastodynamics, can also be generalized to model the collective dynamics of other polar topological structures such as skyrmions. Therefore, the present letter offers a general theoretical framework for understanding and manipulating the structural modes of extended objects in ferroelectric systems.

We thank Venkatraman Gopalan and Jirka Hlinka for helpful discussions and comments on the work. The work is primarily supported as part of the Computational Materials Sciences Program funded by the US Department of Energy, Office of Science, Basic Energy Sciences, under Award No. DE-SC0020145. The authors also acknowledge partial support from the National Science Foundation under Award No. DMR-1744213 for the early effort on the development of dynamical phase-field model, the US Department of Energy under Award No. DE-SC-0012375 on the experimental effort, and computational resource provided by the Institute for CyberScience at the Pennsylvania State University. H.W. acknowledges the support from the US Department of Energy, Office of Science, Basic Energy Sciences, Materials Sciences and Engineering Division.

-
- [1] C. v. Korff Schmising, M. Bargheer, M. Kiel, N. Zhavoronkov, M. Woerner, T. Elsaesser, I. Vrejoiu, D. Hesse, and M. Alexe, Coupled Ultrafast Lattice and Polarization Dynamics in Ferroelectric Nanolayers, *Phys. Rev. Lett.* **98**, 257601 (2007).
 - [2] L. Chen, J.-C. Yang, C.-W. Luo, C. Laing, K.-H. Wu, J.-Y. Lin, T. Uen, J.-Y. Juang, Y. Chu, and T. Kobayashi, Ultrafast photoinduced mechanical strain in epitaxial BiFeO_3 thin films, *Appl. Phys. Lett.* **101**, 041902 (2012).
 - [3] D. Daranciang, M. J. Highland, H. Wen, S. M. Young, N. C. Brandt, H. Y. Hwang, M. Vattilana, M. Nicoul, F. Quirin, J. Goodfellow, T. Qi, I. Grinberg, D. M. Fritz, M. Cammarata, D. Zhu, H. T. Lemke, D. A. Walko, E. M. Dufresne, Y. Li, J. Larsson *et al.*, Ultrafast Photovoltaic Response in Ferroelectric Nanolayers, *Phys. Rev. Lett.* **108**, 087601 (2012).
 - [4] I. Katayama, H. Aoki, J. Takeda, H. Shimosato, M. Ashida, R. Kinjo, I. Kawayama, M. Tonouchi, M. Nagai, and K. Tanaka, Ferroelectric Soft Mode in a SrTiO_3 Thin Film Impulsively Driven to the Anharmonic Regime Using Intense Picosecond Terahertz Pulses, *Phys. Rev. Lett.* **108**, 097401 (2012).
 - [5] M. Lejman, G. Vaudel, I. C. Infante, P. Gemeiner, V. E. Gusev, B. Dkhil, and P. Ruello, Giant ultrafast photo-induced shear strain in ferroelectric BiFeO_3 , *Nat. Commun.* **5**, 4301 (2014).
 - [6] R. Mankowsky, A. von Hoegen, M. Först, and A. Cavalleri, Ultrafast Reversal of the Ferroelectric Polarization, *Phys. Rev. Lett.* **118**, 197601 (2017).
 - [7] X. Li, T. Qiu, J. Zhang, E. Baldini, J. Lu, A. M. Rappe, and K. A. Nelson, Terahertz fieldinduced ferroelectricity in quantum paraelectric SrTiO_3 , *Science* **364**, 1079 (2019).
 - [8] S.-B. Choe, Y. Acremann, A. Scholl, A. Bauer, A. Doran, J. Stöhr, and H. A. Padmore, Vortex core-driven magnetization dynamics, *Science* **304**, 420 (2004).
 - [9] N. Nagaosa and Y. Tokura, Topological properties and dynamics of magnetic skyrmions, *Nat. Nanotechnol.* **8**, 899 (2013).
 - [10] G. Catalan, J. Seidel, R. Ramesh, and J. F. Scott, Domain wall nanoelectronics, *Rev. Mod. Phys.* **84**, 119 (2012).
 - [11] A. K. Yadav, C. T. Nelson, S. L. Hsu, Z. Hong, J. D. Clarkson, C. M. Schlepütz, A. R. Damodaran, P. Shafer, E. Arenholz, L. R. Dedon, D. Chen, A. Vishwanath, A. M. Minor, L. Q. Chen, J. F. Scott, L. W. Martin, and R. Ramesh, Observation of polar vortices in oxide superlattices, *Nature (London)* **530**, 198 (2016).
 - [12] S. Das, Y. L. Tang, Z. Hong, M. A. P. Gonçalves, M. R. McCarter, C. Klewe, K. X. Nguyen, F. Gómez-Ortiz, P. Shafer,

- E. Arenholz, V. A. Stoica, S.-L. Hsu, B. Wang, C. Ophus, J. F. Liu, C. T. Nelson, S. Saremi, B. Prasad, A. B. Mei, D. G. Schlom, J. Íñiguez, P. Garca-Fernández, D. A. Muller, L.-Q. Chen, J. Junquera, L. W. Martin, and R. Ramesh, Observation of room-temperature polar skyrmions, *Nature (London)* **568**, 368 (2019).
- [13] Y. P. Ivanov, A. Chuvilin, L. G. Vivas, J. Kosel, O. Chubykalo-Fesenko, and M. Vázquez, Single crystalline cylindrical nanowires – toward dense 3D arrays of magnetic vortices, *Sci. Rep.* **6**, 23844 (2016).
- [14] A. Fert, N. Reyren, and V. Cros, Magnetic skyrmions: Advances in physics and potential applications, *Nat. Rev. Mater.* **2**, 17031 (2017).
- [15] Q. Li, V. A. Stoica, M. Paciak, Y. Zhu, Y. Yuan, T. Yang, M. R. McCarter, S. Das, A. K. Yadav, S. Park, C. Dai, H. J. Lee, Y. Ahn, S. D. Marks, T. Sato, M. C. Hoffmann, M. Chollet, M. E. Kozina, S. Nelson, D. Zhu *et al.*, Subterahertz collective dynamics of polar vortices, *Nature (London)* **592**, 376 (2021).
- [16] C. Kittel, Domain boundary motion in ferroelectric crystals and the dielectric constant at high frequency, *Phys. Rev.* **83**, 458 (1951).
- [17] G. Arlt and N. A. Pertsev, Force constant and effective mass of 90° domain walls in ferroelectric ceramics, *J. Appl. Phys.* **70**, 2283 (1991).
- [18] G. Wysin, Magnetic vortex mass in two-dimensional easy-plane magnets, *Phys. Rev. B* **54**, 15156 (1996).
- [19] G. Tatara and H. Kohno, Theory of Current-Driven Domain Wall Motion: Spin Transfer Versus Momentum Transfer, *Phys. Rev. Lett.* **92**, 086601 (2004).
- [20] E. Saitoh, H. Miyajima, T. Yamaoka, and G. Tatara, Current-induced resonance and mass determination of a single magnetic domain wall, *Nature (London)* **432**, 203 (2004).
- [21] D. Bedau, M. Kläui, S. Krzyk, U. Rudiger, G. Faini, and L. Vila, Detection of Current-Induced Resonance of Geometrically Confined Domain Walls, *Phys. Rev. Lett.* **99**, 146601 (2007).
- [22] I. Makhfudz, B. Kruger, and O. Tchernyshyov, Inertia and Chiral Edge Modes of a Skyrmion Magnetic Bubble, *Phys. Rev. Lett.* **109**, 217201 (2012).
- [23] F. Büttner, C. Moutafis, M. Schneider, B. Krüger, C. M. Günther, J. Geilhufe, C. v. K. Schmising, J. Mohanty, B. Pfau, S. Schaffert, A. Bisig, M. Foerster, T. Schulz, C. A. F. Vaz, J. H. Franken, H. J. M. Swagten, M. Kläui, and S. Eisebitt, Dynamics and inertia of skyrmionic spin structures, *Nat. Phys.* **11**, 225 (2015).
- [24] J.-M. Hu, T. Yang, K. Momeni, X. Cheng, L. Chen, S. Lei, S. Zhang, S. Trolrier-McKinstry, V. Gopalan, G. P. Carman, C.-W. Nan, and L.-Q. Chen, Fast magnetic domain-wall motion in a ring-shaped nanowire driven by a voltage, *Nano Lett.* **16**, 2341 (2016).
- [25] I. Luk'yanchuk, A. Sene, and V. M. Vinokur, Electrodynamics of ferroelectric films with negative capacitance, *Phys. Rev. B* **98**, 024107 (2018).
- [26] J.-M. Hu, T. Yang, and L.-Q. Chen, Stability and dynamics of skyrmions in ultrathin magnetic nanodisks under strain, *Acta Mater.* **183**, 145 (2020).
- [27] P. Zubko, J. C. Wojde, M. Hadjimichael, S. Fernandez-Pena, A. Sené, I. Lukyanchuk, J.-M. Triscone, and J. Íñiguez, Negative capacitance in multidomain ferroelectric superlattices, *Nature (London)* **534**, 524 (2016).
- [28] See Supplemental Material at <http://link.aps.org/supplemental/10.1103/PhysRevB.103.L220303> for (1) calculation of the inhomogeneous elastic energy function, (2) estimation of the stability of the closed polarization loops, (3) calculation of the elastodynamic contribution to the kinetic energy of the slow mode, (4) numerical solution of the anharmonic oscillator for the slow mode and the effect of energy input, and (5) phase-field simulation of the vortex modes, which includes Refs. [15,29–31,38–40].
- [29] N. A. Pertsev, A. G. Zembilgotov, and A. K. Tagantsev, Effect of Mechanical Boundary Conditions on Phase Diagrams of Epitaxial Ferroelectric Thin Films, *Phys. Rev. Lett.* **80**, 1988 (1998).
- [30] M. J. Haun, E. Furman, S. Jang, H. McKinstry, and L. Cross, Thermodynamic theory of PbTiO₃, *J. Appl. Phys.* **62**, 3331 (1987).
- [31] T. Yang, B. Wang, J.-M. Hu, and L.-Q. Chen, Domain Dynamics Under Ultrafast Electric-Field Pulses, *Phys. Rev. Lett.* **124**, 107601 (2020).
- [32] H. Akamatsu, Y. Yuan, V. A. Stoica, G. Stone, T. Yang, Z. Hong, S. Lei, Y. Zhu, R. C. Haislmaier, J. W. Freeland, L.-Q. Chen, H. Wen, and V. Gopalan, Light-Activated Gigahertz Ferroelectric Domain Dynamics, *Phys. Rev. Lett.* **120**, 096101 (2018).
- [33] M. Foeth, A. Sfera, P. Stadelmann, and P.-A. Buffat, A comparison of HREM and weak beam transmission electron microscopy for the quantitative measurement of the thickness of ferroelectric domain walls, *Microscopy* **48**, 717 (1999).
- [34] W. Cochran, Crystal stability and the theory of ferroelectricity, *Adv. Phys.* **9**, 387 (1960).
- [35] W. Cochran, Dynamical, scattering and dielectric properties of ferroelectric crystals, *Adv. Phys.* **18**, 157 (1969).
- [36] K. Y. Guslienko, B. Ivanov, V. Novosad, Y. Otani, H. Shima, and K. Fukamichi, Eigenfrequencies of vortex state excitations in magnetic submicron-size disks, *J. Appl. Phys.* **91**, 8037 (2002).
- [37] P. Warnicke, P. Wohlhuter, A. K. Suszka, S. E. Stevenson, L. J. Heyderman, and J. Raabe, Tunable magnetic vortex resonance in a potential well, *Phys. Rev. B* **96**, 174402 (2017).
- [38] J. B. Goodenough, Interpretation of domain patterns recently found in BiMn and SiFe alloys, *Phys. Rev.* **102**, 356 (1956).
- [39] C. Kittel, Physical theory of ferromagnetic domains, *Rev. Mod. Phys.* **21**, 541 (1949).
- [40] G. Sheng, Y. Li, J. Zhang, S. Choudhury, Q. Jia, V. Gopalan, D. G. Schlom, Z.-K. Liu, and L.-Q. Chen, A modified Landau-Devonshire thermodynamic potential for strontium titanate, *Appl. Phys. Lett.* **96**, 232902 (2010).